Report

Neuron

Dynamic, Cell-Type-Specific Roles for GABAergic Interneurons in a Mouse Model of Optogenetically Inducible Seizures

Highlights

- We describe a novel protocol for reliable optogenetic induction of seizures
- Seizure-related interneuron activity precedes that of excitatory neurons
- Inhibiting VIP+ interneurons disrupts seizure initiation and maintenance
- The effects of inhibiting PV+ and SOM+ interneurons vary as seizures evolve

Authors

Sattar Khoshkhoo, Daniel Vogt, Vikaas S. Sohal

Correspondence

vikaas.sohal@ucsf.edu

In Brief

Khoshkhoo et al. describe a mouse model for optogenetic seizure induction. Combining this model with Ca^{2+} imaging and optogenetic inhibition, they find evolving roles for PV+ and SOM+ interneurons during seizures and identify VIP+ interneurons as targets for seizure control.

Khoshkhoo et al., 2017, Neuron *93*, 1–8
January 18, 2017
http://dx.doi.org/10.1016/j.neuron.2016.11.043

CellPress

Please cite this article in press as: Khoshkhoo et al., Dynamic, Cell-Type-Specific Roles for GABAergic Interneurons in a Mouse Model of Optogenetically Inducible Seizures, Neuron (2016), http://dx.doi.org/10.1016/j.neuron.2016.11.043

Neuron
Report

Dynamic, Cell-Type-Specific Roles for GABAergic Interneurons in a Mouse Model of Optogenetically Inducible Seizures

Sattar Khoshkhoo,[1,2,3,4] Daniel Vogt,[1,2,3] and Vikaas S. Sohal[1,2,3,4,5,*]
[1]Department of Psychiatry
[2]Weil Institute for Neurosciences
[3]Kavli Institute for Fundamental Neuroscience
[4]Sloan Swartz Center for Theoretical Neurobiology
University of California, San Francisco, San Francisco, CA 94143-0444, USA
[5]Lead Contact
*Correspondence: vikaas.sohal@ucsf.edu
http://dx.doi.org/10.1016/j.neuron.2016.11.043

SUMMARY

GABAergic interneurons play critical roles in seizures, but it remains unknown whether these vary across interneuron subtypes or evolve during a seizure. This uncertainty stems from the unpredictable timing of seizures in most models, which limits neuronal imaging or manipulations around the seizure onset. Here, we describe a mouse model for optogenetic seizure induction. Combining this with calcium imaging, we find that seizure onset rapidly recruits parvalbumin (PV), somatostatin (SOM), and vasoactive intestinal peptitde (VIP)-expressing interneurons, whereas excitatory neurons are recruited several seconds later. Optogenetically inhibiting VIP interneurons consistently increased seizure threshold and reduced seizure duration. Inhibiting PV+ and SOM+ interneurons had mixed effects on seizure initiation but consistently reduced seizure duration. Thus, while their roles may evolve during seizures, PV+ and SOM+ interneurons ultimately help maintain ongoing seizures. These results show how an optogenetically induced seizure model can be leveraged to pinpoint a new target for seizure control: VIP interneurons.

INTRODUCTION

Epilepsy has many genetic (Mantegazza et al., 2010) and acquired (Shorvon, 2011) causes. For almost all of these, GABAergic interneurons play critical roles in regulating the activity of cortical microcircuits implicated in seizures and epilepsy (Paz and Huguenard, 2015). Nevertheless, the exact role of GABAergic interneurons in seizure initiation, propagation, maintenance, and termination is still debated. Studies in mice have shown that enhancing interneuron output, by either transplanting medial ganglionic eminence (MGE)-derived interneuron precursors (Hunt et al., 2013) or optogenetically activating parvalbumin-expressing (PV+) interneurons (Krook-Magnuson et al., 2013), can decrease seizure frequency or promote seizure termination. Whereas these findings support a role for interneurons in suppressing seizures, other studies have proposed that interneurons could contribute to excessive neuronal synchronization in ways that promote seizures (Alvarado-Rojas et al., 2013; Ellender et al., 2014). One mechanism through which interneurons may contribute to seizures is by eliciting depolarizing GABAergic currents (Alger and Nicoll, 1979; Andersen et al., 1980; Perreault and Avoli, 1992). Thus, whereas it is clear that under certain conditions, increasing interneuron output suppresses seizures, it remains unclear whether this is always the case, or whether interneurons can at times act to promote seizures.

Further complicating matters, cortical GABAergic interneurons comprise numerous heterogeneous subtypes, and the roles of many of these remain unknown. Unlike MGE-derived PV+ and somatostatin-expressing (SOM+) interneurons, whose roles in seizures have frequently been studied (Paz and Huguenard, 2015), little is known about the contribution of a distinct population of interneurons that express vasoactive intestinal peptide (VIP). VIP+ interneurons are believed to synapse primarily onto other GABAergic interneurons and play a disinhibitory role in cortical circuits (Lee et al., 2013; Pi et al., 2013). Three observations suggest a possible role for VIP+ interneurons in seizures: VIP levels are increased in the CSF of children with chronic epilepsy (Ko et al., 1991); levels of VIP receptor binding are increased in post-mortem tissue from individuals with temporal lobe epilepsy (de Lanerolle et al., 1995); and VIP+ interneuron firing increases as spike and wave discharges develop in tubocurarine-treated rat cortical slices (Hall et al., 2015). Nevertheless, the significance of these findings remains unknown.

Some of the uncertainty around the role of interneurons stems from the fact that in vivo, systems-level investigations of seizures have been challenging. This is largely because most in vivo models of chronic epilepsy develop spontaneous seizures (Raol and Brooks-Kayal, 2012). This lack of temporal control over seizure onset limits the use of advanced imaging and cellular manipulation techniques, such as Ca^{2+} imaging and optogenetics.

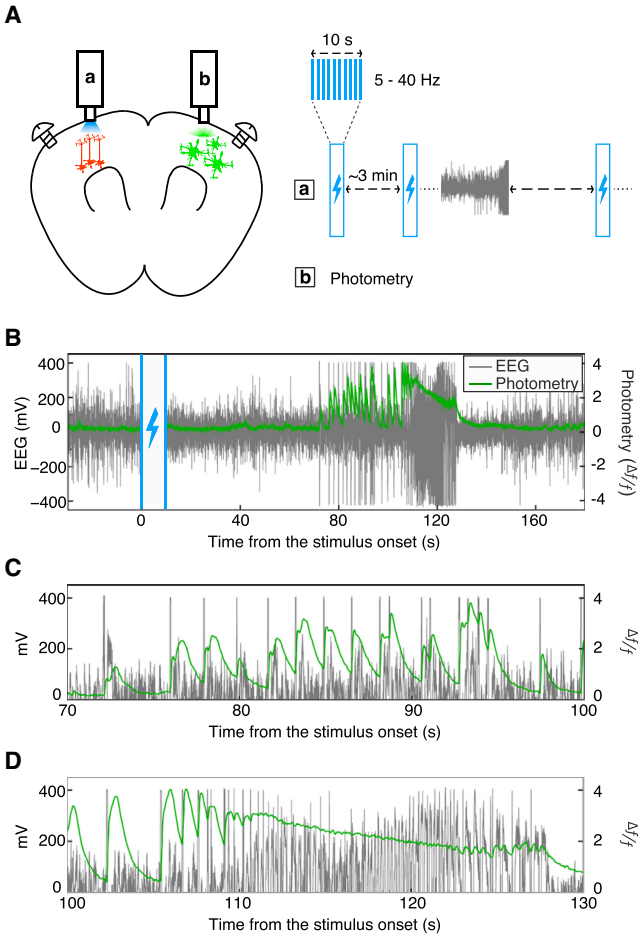

Figure 1. Simultaneous EEG Recording and Bulk Calcium Imaging in a Mouse Model for Optogenetically Inducible Seizures

(A) Schematic illustrating the experimental design for optogenetic seizure induction as well as simultaneous EEG recording and photometry. For seizure induction, blue light was delivered through cannula a. For photometry, bulk fluorescence from neurons expressing GCaMP6f was captured through cannula b. Bilateral EEG was recorded via skull screws.

(B) Example of simultaneous EEG and photometry recordings during a seizure in a SOM-Cre mouse. Time 0 marks the onset of the stimulus immediately preceding the seizure.

(C) Example of simultaneous EEG and photometry recordings from (B), zoomed in to illustrate the high correlation between the electrographic seizure activity and photometry signals.

(D) Example of simultaneous EEG and photometry recordings from (B), zoomed in to illustrate the temporal limitation of photometry in discerning individual epileptiform discharges at high frequencies.

See also Figure S1.

Here, we address some of these issues by first developing an in vivo optogenetically inducible mouse model of ictogenesis that captures key features of clinically observed seizures. We then use this model together with cell-type-specific bulk Ca^{2+} imaging to measure the activity patterns of specific classes of interneurons and excitatory neurons during seizures. Finally, we use targeted optogenetic inhibition in this model to show that VIP+ and MGE-derived (PV+ and SOM+) interneurons play different roles in seizures.

RESULTS

Optogenetic Seizure Induction

To induce seizures optogenetically, we used a novel protocol combining multiple stimulation frequencies and light intensities to focally activate ChR2 in the mouse primary motor cortex (Experimental Procedures; Figure 1A). Significantly more seizures occurred following high- (20–40 Hz) versus low- (5–10 Hz) frequency stimulation ($p < 0.001$ by ANOVA; $p < 0.05$ for 20 and 40 Hz versus 5 and 10 Hz stimulation by Tukey-Kramer [TK] multiple comparisons test; Figure S1I). On average, 10–15 optical stimuli were required to induce the first seizure; however, this varied slightly depending on mouse genotype ($p < 10^{-6}$ by ANOVA; n = 4–6 mice for each genotype; Figure S1E). After the first seizure, the probability of seizure induction with each subsequent stimulus was consistently >70%. We did not observe seizures in the absence of a stimulus, even after optogenetic seizure induction. Interestingly, the onset of electrographic and behavioral seizure activity was delayed by 1–2 min following the delivery of each stimulus (Figure S1A). The number of stimuli required to elicit the initial seizure was specific to each mouse and did not change significantly across 3 days of experimentation ($p = 0.27$ by ANOVA; Figure S1F).

Based on electrographic criteria alone (Experimental Procedures), the majority of seizures (79% ± 5%) were primarily generalized at onset, i.e., no initial seizure focus could be identified (Figure S1J). The remaining seizures were mainly focal with secondary generalization (18% ± 2%); a select few were focal (3% ± 3%) (Figure S1J). Interestingly, when an electrographic focus could be identified, it was more often (65% ± 15%) *contralateral* to the site of ChR2 stimulation. Optogenetically induced seizures typically began as bilateral periodic discharges that first evolved into bursts, then into high-frequency, high-amplitude spikes that terminated spontaneously (Figures S1B–S1D). The majority of seizures in all genotypes ranged from stage 3 (unilateral and bilateral limb clonus) to stage 5 (generalized clonic seizures) on a modified Racine scale (Experimental Procedures; Figure S1K). The average seizure duration was 64 ± 6 s and there were no significant differences in duration across genotypes ($p = 0.89$ via ANOVA; n = 19–47 seizures for each genotype; Figure S1G), or the 3 days of experimentation ($p = 0.35$ by ANOVA; n = 31, 43, and 39 seizures on days 1, 2, and 3; Figure S1H).

Cell-Type-Specific Bulk Calcium Imaging

We combined our optogenetic seizure model with fiber photometry (Cui et al., 2014; Gunaydin et al., 2014) to perform cell-type-specific bulk Ca^{2+} imaging during seizures (Experimental Procedures; Figure 1A). We used PV-Cre, SOM-Cre, and VIP-Cre mice to label the major classes of cortical GABAergic interneurons, and Emx1-Cre mice to target the majority of excitatory neurons in neocortex. During each recording session, we optogenetically induced seizures, as described above, while simultaneously recording electrical signals via electroencephalogram (EEG) and Ca^{2+} signals via fiber photometry.

Seizures produced large Ca^{2+} signals in all studied cell types—normalized signals (ΔF/F) were ~1- to 3-fold higher than baseline (Figure 1B; Figures S2A–S2D). Ca^{2+} signals were highly correlated with individual low-frequency electrographic discharges

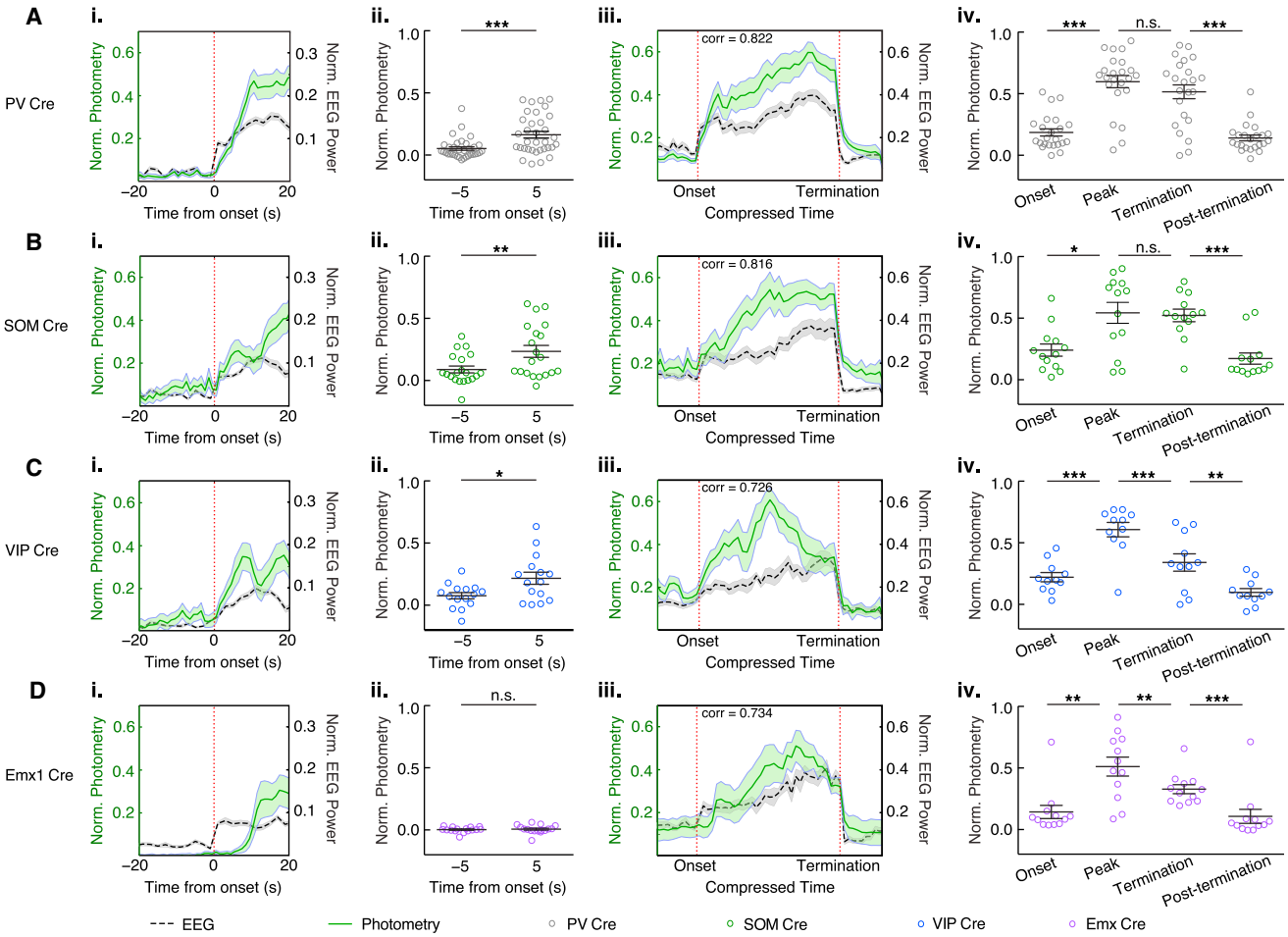

Figure 2. Interneurons and Excitatory Neurons Exhibit Distinct Patterns of Activity during Seizures

(A) (i) Mean EEG power—normalized to the peak EEG power during each seizure—and photometry signals—normalized to the peak photometry signal during each seizure—in PV Cre mice. Both recordings are aligned to the time of seizure onset (indicated by the dotted red line). (ii) Normalized photometry signals 5 s before and after seizure onset. (iii) EEG power and photometry signals with compressed time, aligned to the time of seizure onset and seizure termination. Seizure onset and termination are indicated by the dotted red lines. (iv) Scatterplots showing photometry signals from individual seizures immediately after seizure onset (onset), at the peak—the same data point for all seizures—of the mean photometry trace (peak), one data point prior to seizure termination (termination), and 1 s after seizure termination (post-termination).

(B) Same as (A), but for SOM-Cre mice.

(C) Same as (A), but for VIP-Cre mice.

(D) Same as (A), but for Emx1-Cre mice.

All data show means ± SEM and are analyzed using the two-tailed paired-sample t test. Shading in the traces are ±SEM. Not significant (n.s.), *$p < 0.05$, **$p < 0.01$, ***$p < 0.001$. See also Figures S2 and S3.

in the ipsilateral EEG recording (Figure 1C). Individual Ca^{2+} transients associated with higher-frequency EEG spikes (>5 Hz) could not be resolved, presumably due to the kinetics of GCaMP6f (Figure 1D).

Interneurons and Excitatory Neurons Exhibit Unique Patterns of Activity during Seizures

To compare the activity of different cell types around seizure initiation, we identified the time of electrographic seizure onset, then aligned and averaged all EEG and photometry recordings (Experimental Procedures). The averaged traces show that in PV+, SOM+, and VIP+ interneurons, Ca^{2+} signals increased sharply upon seizure onset (Figures 2Ai, 2Bi, and 2Ci). In contrast, in Emx1+ neurons, the rise in Ca^{2+} signals was delayed by ~10 s following seizure onset (Figure 2Di). To quantify this, we compared Ca^{2+} signals 5 s before versus 5 s after seizure onset for each cell type (Figures 2Aii–2Dii). Ca^{2+} signals after seizure onset were significantly greater than 5 s before seizure onset for all three interneuron subtypes, but not for EMX1+ neurons ($p < 0.001$–0.01 for PV-Cre, SOM-Cre, and VIP-Cre; $p = 0.66$ for Emx1-Cre by two-tailed paired t test; n = 15–34 seizures for each genotype). Importantly, Ca^{2+} signals in EMX1+ neurons were not weaker than those in interneurons (Figures S2A–S2D). Also, the averaged aligned EEG traces demonstrated a similar,

sharp rise in normalized power at the time of seizure onset for all Cre lines (Figures 2Ai–2Di). Thus, these differences in Ca^{2+} signals at the time of seizure onset are not simply artifacts of differences in the seizure dynamics between EMX1-Cre mice and other genotypes.

To compare the activity of different cell types during seizure maintenance and around seizure termination, we created the compressed time plots shown in Figures 2Aiii–2Diii. Each compressed time plot was aligned to both seizure initiation and seizure termination, making it possible to compare mean EEG and photometry signals from seizures with different durations. Based on these plots, Ca^{2+} signals in PV+ and SOM+ neurons increase after seizure onset, then remain maximal until seizure termination (Figures 2Aiii and 2Biii). By contrast, Ca^{2+} signals in VIP+ and Emx1+ neurons appear to peak mid-seizure, then decline before seizure termination (Figures 2Ciii and 2Diii). Again, to quantify these observations, we compared Ca^{2+} signals for each genotype at the following time points: first data point (in compressed time) after seizure onset, at the peak of the trace, first data point (compressed time) prior to seizure termination, and 1 s after seizure termination (Figures 2Aiv–2Div). For every cell type, the peak Ca^{2+} signal during the seizure was significantly greater than at seizure onset ($p < 10^{-6}$–0.05; n = 11–23 seizures for each genotype), and Ca^{2+} signals were greater at the electrographic seizure termination than the post-termination time point ($p < 10^{-6}$–0.001). However, for VIP+ and Emx1+ neurons, the peak Ca^{2+} signal was also significantly greater than the Ca^{2+} signal at seizure termination (VIP: $p < 10^{-4}$, Emx: $p < 0.05$), indicating that Ca^{2+} signals in VIP+ and Emx1+ neurons decrease well before seizure termination. By contrast, for PV+ and SOM+ neurons, Ca^{2+} signals at termination were not significantly different from their peak values.

Notably, all three interneuron Cre lines had high specificity (PV-Cre: 95% ± 1%, SOM-Cre: 84% ± 2%, VIP-Cre: 77% ± 1%; Figures S2E–S2G) and reasonable sensitivity (PV-Cre: 65% ± 4%, SOM-Cre: 49% ± 9%, VIP-Cre: 63% ± 4%; Figures S2E–S2G) for GCaMP expression. No GABAergic interneurons were labeled with GCaMP in Emx1-Cre mice (Figure S2H).

To investigate how specific cell populations contribute to electrographic signals at seizure onset, we attempted to disrupt local field potentials (LFPs) associated with seizures using cell-type-specific optogenetic inhibition. To our surprise, neither specific inhibition of PV+, SOM+, or Emx1+ neurons nor inhibition of *all* neurons using a synapsin promoter attenuated electrographic seizure activity (n = 2–6 mice for each case; Figures S3H–S3K). Importantly, in Emx1-Cre mice, LFPs at the cannula implantation site increased immediately upon seizure onset (n = 2 mice and 5 seizures; Figure S2I). This reaffirms that the delayed increase of Ca^{2+} signals in excitatory cells after seizure onset cannot be attributed to the absence of local electrographic seizure activity, but rather reflects the specific absence of neuronal activity in excitatory neurons.

Using Optogenetic Inhibition to Test Causal Roles for Interneurons in Seizures

We used eArch3.0 to selectively inhibit VIP+ interneurons, Dlx12b-labeled interneurons, PV+ interneurons, or SOM+ interneurons during optogenetically induced seizures (Figure 3A; Figures S3A–S3C and S3L). Dlx12b labels 80%–90% of PV+ and SOM+ interneurons and far fewer calretinin (CR)+ interneurons, a small subset of which are VIP+ (Potter et al., 2009). First, we looked at the effects of interneuron inhibition during the preictal phase. Inhibiting VIP+ interneurons *contralateral* (but not ipsilateral) to the stimulation site significantly increased seizure threshold, shown by a rightward shift of the cumulative probability distribution for seizure probability versus number of stimuli ($p < 10^{-8}$ between baseline and contra via TK multiple comparisons test; n = 5 mice; Figure 3C). Similarly, the number of optogenetic stimuli required to induce the first seizure increased with inhibition of VIP+ interneurons contralateral to the stimulation site ($p < 0.05$ via two-tailed t test; n = 5 mice; Figure 3D). Importantly, there was no significant change in seizure threshold in control mice expressing eYFP in VIP+ interneurons across 3 days of experimentation (ipsilateral: p = 0.82, contralateral: p = 0.16 by two-tailed t test; n = 4 mice; Figure 3D).

In contrast, inhibiting Dlx12b+ interneurons, both ipsilateral and contralateral to the stimulation site, *decreased* seizure threshold (ipsilateral: $p < 0.01$, contralateral: $p < 0.001$ via TK multiple comparisons test; n = 7 mice; Figure 3B). Both ipsilateral and contralateral inhibition of Dlx12b+ interneurons decreased the number of stimuli needed to elicit the first seizure (ipsilateral: $p < 0.05$; contralateral: $p < 0.01$ by two-tailed t test; n = 7 mice; Figure 3D).

Repeating this experiment using more specific PV-Cre and SOM-Cre mouse lines yielded more complex results. Ipsilateral and contralateral inhibition of SOM+ interneurons alone had no effect on seizure probability (p = 0.75–0.98 by TK multiple comparisons test; n = 4 mice; Figure S3E) or seizure threshold (ipsilateral: p = 0.55–0.63 by two-tailed t test; n = 4 mice; Figure S3F). Contralateral inhibition of PV+ interneurons actually decreased seizure probability ($p < 0.05$ between baseline and contra via TK multiple comparisons test; n = 6 mice; Figure S3D) and increased seizure threshold ($p < 0.05$ by two-tailed t test; Figure S3F). Ipsilateral PV+ inhibition had negligible effects (Figures S3D and S3F).

We also analyzed the effects of interneuron inhibition on seizure maintenance and termination. Consistent with the antiseizure effects of inhibiting VIP+ interneurons on seizure initiation, we found that inhibiting VIP+ interneurons contralateral to the stimulation site shortened seizure duration ($p < 0.01$ by two-tailed t test; n = 5 mice; Figure 3E). Surprisingly, in stark contrast to the pro-seizure effects of inhibiting Dlx12b+ interneurons during seizure initiation, inhibition of Dlx12b+ interneurons either ipsi- or contralateral to the stimulation site significantly *reduced* seizure length (ipsilateral: $p < 10^{-6}$, contralateral $p < 0.001$ by two-tailed t test; n = 7 mice; Figure 3E).

Consistent with the reduced seizure duration observed after inhibiting Dlx12b+ interneurons, both ipsilateral and contralateral inhibition of SOM+ interneurons alone reduced seizure duration (ipsilateral: $p < 10^{-5}$, contralateral: $p < 0.05$ by two-tailed t test; n = 4 mice; Figure S3G). Contralateral inhibition of PV+ interneurons also reduced seizure duration ($p < 0.01$; n = 6 mice; Figure S3G); ipsilateral inhibition of PV+ interneurons elicited a borderline-significant reduction in seizure duration (ipsilateral: p = 0.06; n = 6 mice; Figure S3G). Again, there was no significant change in seizure duration in control mice expressing eYFP in

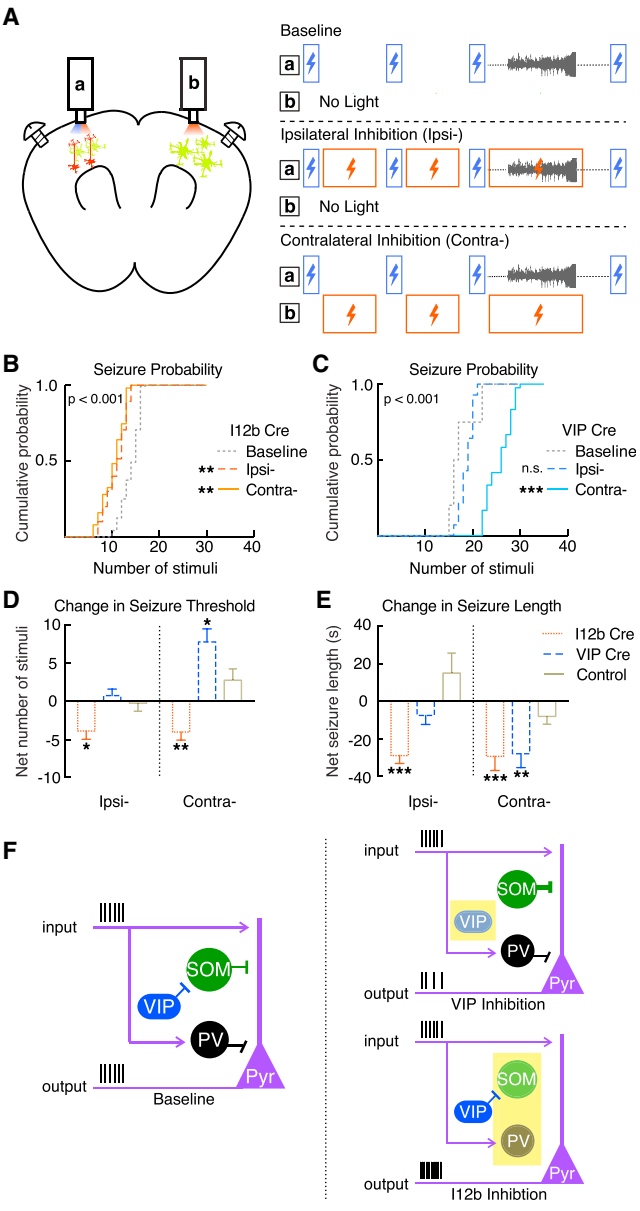

Figure 3. Cell-Type-Specific Optogenetic Inhibition Reveals Different Roles for DlxI12b+ and VIP+ Interneurons in Seizure Initiation and Maintenance

(A) Schematic illustrating the design of experiments using optogenetic inhibition of interneurons. For seizure induction, 445 nm light was delivered through cannula a using the same protocol shown in Figure 1. Interneuron inhibition was achieved by delivering a constant 594 nm amber light through cannula a or b. Experiments were performed on 3 consecutive days using three different conditions, as shown. Bilateral EEG was recorded via skull screws.

(B and C) Cumulative probability for seizure induction as a function of the number of optogenetic stimuli delivered in DlxI12b-Cre (B) and VIP-Cre (C) mice. "ipsi" and "contra" refer to inhibition of ipsilateral or contralateral interneurons, respectively, as shown in (A).

(D) Change in the number of stimuli required to induce the first seizure (seizure threshold) relative to baseline.

(E) Change in seizure duration relative to baseline.

(F) Schematic illustrating a simplified model for cortical microcircuits comprising interneurons and excitatory neurons during the pre-ictal stage. Arrows and flat lines symbolize excitatory and inhibitory synapses, respectively. Yellow boxes illustrate optogenetic inhibition.

All data show means ± SEM. Data in (B) and (C) are analyzed using one-way ANOVA and multiple comparisons test and data in (D) and (E) are analyzed using two-tailed Student's t test. In (D) and (E), unless marked on the figure, there are no significant changes. Not significant (n.s.), *p < 0.05, **p < 0.01, ***p < 0.001.

VIP+ interneurons across 3 days of experimentation (n = 4 mice; Figure 3E).

Post-ictal EEG Depression Is Associated with Cortical Spreading Depression-like Events

52% ± 7% of seizures were associated with large, prolonged (~1–2 min) increases in Ca^{2+} signals, almost always after seizure termination, which resembled cortical spreading depression (CSD) (Figures 4A and 4B). During these events, the EEG electrode closest to the photometry site typically exhibited a broadband decrease in power (Figure 4C). The reduction in EEG power was localized—EEG power was significantly higher on the contralateral side ($p < 0.001$ for all genotypes/cell types, n = 9–29 events for each genotype; Figures S4B–S4E). These characteristics, i.e., a localized reduction in electrical activity that coincides with a strong increase in Ca^{2+} signals and lasts ~1–2 min, are consistent with post-ictal depression and also match those recently reported by a study of CSD that also used GCaMP imaging (Enger et al., 2015). CSD-like events did not happen in the absence of seizures and almost always followed seizure termination (Figure 4D). However, some CSD-like events could precede seizure termination. Interestingly, these resulted in a dramatic reduction in the power of electrographic seizure activity (Figure S4A).

CSD-like events were similar in photometry measurements from different cell types. There was no difference in event length ($p = 0.13$ via ANOVA; Figure 4E) or onset time relative to seizure termination ($p = 0.99$ by ANOVA; Figure 4D). The time from event onset to peak was significantly longer in Emx1+ neurons compared to interneurons ($p < 0.001$ for PV-Cre versus Emx-1-Cre, $p < 0.01$ for SOM-Cre versus Emx1-Cre, $p < 0.001$ for VIP-Cre versus Emx1-Cre via TK multiple comparisons test; Figure 4F).

DISCUSSION

We developed an optogenetic model for inducing seizures in awake, freely moving mice. Using this model, we performed cell-type-specific Ca^{2+} imaging and optogenetic inhibition to elucidate roles of interneurons in various stages of seizures. Seizures recruit interneurons within <1 s of seizure onset, whereas the recruitment of excitatory neurons follows after a delay of ~10 s. Furthermore, Ca^{2+} signals in PV+ and SOM+ interneurons remain maximal until seizure termination, whereas Ca^{2+} signals in VIP+ interneurons and excitatory neurons begin to decrease well before the end of the electrographic seizure. During the pre-ictal period, inhibiting PV+ and SOM+ interneurons could either increase or decrease the seizure threshold, depending on whether they were inhibited selectively (using PV- and SOM-Cre mice), or simultaneously (using DlxI12b-Cre mice).

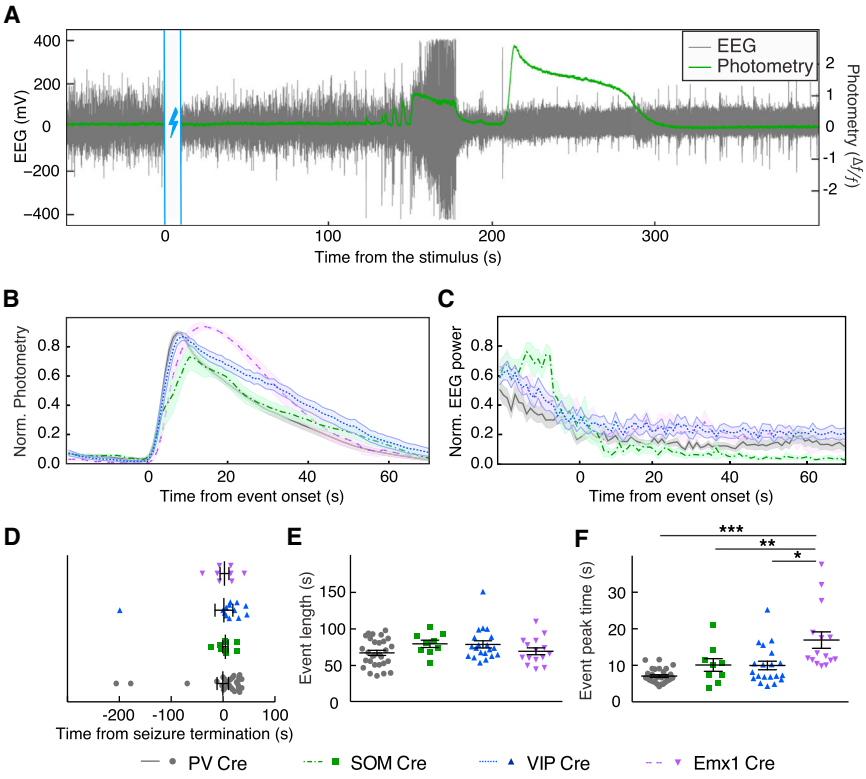

Figure 4. Cortical Spreading Depression-like Events Associated with Seizures

(A) Example of simultaneous EEG and photometry recordings in a PV-Cre mouse demonstrating a cortical spreading depression (CSD)-like event during the post-ictal period. Time 0 marks the onset of the stimulus immediately preceding the seizure.

(B) Mean photometry recordings—normalized to the peak of each CSD-like event—aligned to the onset of the CSD-like events.

(C) Mean EEG power aligned to the onset of the CSD-like events.

(D) Time of onset of each CSD-like event, relative to the time of termination of each seizure. Each data point is derived from a single seizure.

(E) Duration of CSD-like events. Each data point is derived from a single seizure.

(F) Time from the onset to the peak of each CSD-like event. Each data point is derived from a single seizure.

All data show means ± SEM and are analyzed using one-way ANOVA and multiple comparisons test. Shading in the traces and error bars in the scatterplots are ±SEM. In (D) through (G), unless marked on the figure, there are no significant differences between different genotypes. $^{**}p < 0.01$, $^{***}p < 0.001$. See also Figure S4.

However, during the ictal stage, inhibiting PV+ and/or SOM+ interneurons consistently prolonged seizures. By contrast, inhibiting VIP+ interneurons increased the threshold for seizure initiation and decreased seizure length, suggesting that these interneurons are consistently disinhibitory and pro-seizure.

An Optogenetic Mouse Model for Seizures

The optogenetic model for seizure induction described here may complement other models of seizures. In contrast to traditional electrical kindling models (Raol and Brooks-Kayal, 2012), optogenetic seizure induction occurs relatively rapidly and the threshold for seizure induction returns to baseline each day. This makes it possible to design experiments that span multiple days in order to compare the effects of different manipulations (e.g., the optogenetic inhibition of interneurons used here). Moreover, seizures occur at a stereotyped delay (~1–2 min) following the stimulus, creating a window of opportunity for imaging and/or cellular manipulation prior to seizure initiation.

Interestingly, optogenetically evoked seizures were often followed by events that had features consistent with both post-ictal EEG depression and cortical spreading depression. Notably, previous studies have implicated Ca^{2+} influx in post-ictal hyperpolarization (Lopantsev and Taranenko, 1990).

The Function of PV+ and SOM+ Interneurons during Seizure Initiation

We found that interneurons are rapidly recruited at seizure onset. This finding is consistent with previous work showing pre-ictal increases in the synchrony (Grasse et al., 2013) and firing rate (Toyoda et al., 2015) of interneurons in pilocarpine-treated rats and a patient with focal epilepsy (Truccolo et al., 2011). Notably, the recruitment of interneurons precedes that of excitatory neurons by several seconds. There are two possible explanations for this observation. One is that the rapid recruitment of interneurons results, at least transiently, in reduced local excitability (Bragin et al., 2005) and decreased principal cell firing (Bower and Buckmaster, 2008). Another possibility is that interneurons contribute to seizure initiation. We found evidence for both scenarios. Silencing a large population of DlxI12b-labeled PV+ and SOM+ interneurons significantly reduced seizure threshold, consistent with the idea that a global reduction in inhibition makes seizures more likely. However, when we selectively inhibited smaller populations of PV+ and SOM+ interneurons, we observed either no effect on seizure threshold (in SOM-Cre mice), or an increase in seizure threshold (in PV-Cre mice).

Why did we observe different effects on seizure threshold—no change, an increase, or a decrease—in SOM-Cre, PV-Cre, and DlxI12b-Cre mice, respectively? Although the use of PV-Cre and SOM-Cre mice to selectively label PV+ or SOM+ interneurons has excellent specificity, the sensitivity is more modest (Figures S2E and S2F). This is a particular concern for PV+ and SOM+ interneurons given their high degree of interconnectivity. Because of this, inhibiting only a subset of PV or SOM interneurons might actually *disinhibit* many remaining interneurons. By contrast, DlxI12b-Cre mice label the majority of both cortical PV+ and SOM+ interneurons (Potter et al., 2009), making them less susceptible to this potential issue. With this in mind, the discordant effects we observed on seizure threshold may reflect

differences in the ability of various manipulations to disrupt overall levels of circuit inhibition. Alternatively, differences in genetic background may explain why inhibiting interneurons has different effects on seizure threshold in PV-Cre, SOM-Cre, and Dlx12b-Cre mice.

The Function of PV+ and SOM+ Interneurons during Seizure Maintenance

We also examined whether interneurons play the same or different roles during seizure maintenance and termination compared to seizure initiation. PV+ and SOM+ interneurons maintain high Ca^{2+} signals until seizure termination, suggesting strong interneuron recruitment during seizures. Our observations that inhibiting PV+ and/or SOM+ interneurons, either selectively or at the same time (using Dlx12b-Cre mice) consistently reduces seizure duration suggests that these interneurons play an important role in seizure maintenance during the ictal stage. PV+ interneurons may contribute to this process (Ellender et al., 2014) by recruiting depolarizing GABAergic synaptic potentials (Alger and Nicoll, 1979; Andersen et al., 1980; Perreault and Avoli, 1992). It is possible that intense ongoing synaptic activity over the course of a seizure drives intracellular chloride accumulation by causing a shift in the reversal potential (Arellano et al., 2004; Staley et al., 1995).

VIP+ Interneurons Maintain a Disinhibitory Role throughout the Seizure

Previous studies have shown that mice with reduced numbers of VIP+ interneurons are "seizure resistant" (Lodato et al., 2011) and bath application of a VIP receptor antagonist can decrease the incidence of acute tubocurarine-induced spike and wake discharges in rat cortical slices (Hall et al., 2015). These observations are in agreement with the hypothesis that VIP+ interneurons have a predominately disinhibitory role in cortical circuits (Lee et al., 2013; Pi et al., 2013). Consistent with this, we found that preictal inhibition of VIP+ interneurons significantly increased the threshold for optogenetic seizure induction. Additionally, ictal inhibition of VIP+ interneurons decreased seizure length. These findings demonstrate that inhibition of VIP+ interneurons has a consistent anti-seizure effect (Figure 3F). This effect should be tested in models of chronic epilepsy and could be exploited for the development of new antiepileptic treatments.

Limitations and Future Directions

For seizure induction, we expressed ChR2 under control of the commonly used CaMKIIα 1.3 promoter, which is only 82% specific for excitatory neurons (Scheyltjens et al., 2015). Thus, it would be informative to explore how optogenetic stimulation of specific neuronal subpopulations contributes to seizure induction. Our study also relies on photometry, which enables cell-type-specific activity measurements in freely moving mice but is limited by the temporal resolution of existing GCaMP sensors and lacks spatial resolution. Other imaging methods, e.g., two-photon microscopy or microendoscopy could add additional details about interactions between individual neurons.

Additionally, our findings rely on the assumption that intracellular Ca^{2+} reliably indicates neuronal activity. While the bevy of recent studies using similar approaches underscore the presumption that this is generally valid, GCaMP imaging cannot distinguish neuronal firing from other possible drivers of Ca^{2+} influx. Nevertheless, an important observation is that the magnitudes of signals, e.g., peak amplitudes of $\Delta F/F$, were broadly similar in excitatory and inhibitory neurons, suggesting that differences in these signals do not simply reflect cell-type differences in the sensitivity of GCaMP sensors.

Puzzlingly, we were unable to identify the source of LFPs using cell-type-specific optogenetic inhibition. A possible explanation is that the spatial extent of optogenentic inhibition is relatively small. As such, cell-type-specific inhibitory tools with broader spatial coverage, e.g., DREADDs, would be interesting to use in the future.

As discussed above, PV+ and/or SOM+ interneurons may help maintain seizures by recruiting depolarizing GABAergic currents following the intracellular accumulation of chloride. Future studies could evaluate this directly using the genetically encoded chloride indicator, Clomeleon (Kuner and Augustine, 2000), together with photometry (Wells et al., 2016) to measure intracellular chloride changes during seizures.

Finally, although our optogenetic model for seizure induction allowed us to overcome certain experimental challenges, it does not reproduce the spontaneous seizures that occur in chronic epilepsy. Thus, optogenetic seizure induction is best thought of as an adjunctive tool, which complements genetic and pharmacologic models of epilepsy. Future studies should both revisit our findings using well-validated models of epilepsy, and validate the effects of anticonvulsant drugs in optogenetic seizure model.

EXPERIMENTAL PROCEDURES

Full Experimental Procedures are in the Supplemental Experimental Procedures.

SUPPLEMENTAL INFORMATION

Supplemental Information includes Supplemental Experimental Procedures and four figures and can be found with this article online at http://dx.doi.org/10.1016/j.neuron.2016.11.043.

AUTHOR CONTRIBUTIONS

S.K. performed the experiments. D.V. performed immunohistochemistry. S.K. and V.S.S. designed the experiments and wrote the paper.

ACKNOWLEDGMENTS

We thank Daniel Lowenstein and Jeanne Paz for helpful comments on the manuscript, K. Cho, M. Cunniff, J. Iafrati, and A. Lee for assistance with slice electrophysiology, and R. Mayeda for scoring seizures. S.K. was supported by the HHMI Medical Research Fellows Program and Citizens United for Research in Epilepsy (CURE). V.S.S. was supported by NIMH (U01MH105948) and the NIH Office of the Director (DP2MH100011).

Received: March 29, 2016
Revised: August 5, 2016
Accepted: November 16, 2016
Published: December 29, 2016

REFERENCES

Alger, B.E., and Nicoll, R.A. (1979). GABA-mediated biphasic inhibitory responses in hippocampus. Nature *281*, 315–317.

Alvarado-Rojas, C., Lehongre, K., Bagdasaryan, J., Bragin, A., Staba, R., Engel, J., Jr., Navarro, V., and Le Van Quyen, M. (2013). Single-unit activities during epileptic discharges in the human hippocampal formation. Front. Comput. Neurosci. *7*, 140.

Andersen, P., Dingledine, R., Gjerstad, L., Langmoen, I.A., and Laursen, A.M. (1980). Two different responses of hippocampal pyramidal cells to application of gamma-amino butyric acid. J. Physiol. *305*, 279–296.

Arellano, J.I., Muñoz, A., Ballesteros-Yáñez, I., Sola, R.G., and DeFelipe, J. (2004). Histopathology and reorganization of chandelier cells in the human epileptic sclerotic hippocampus. Brain *127*, 45–64.

Bower, M.R., and Buckmaster, P.S. (2008). Changes in granule cell firing rates precede locally recorded spontaneous seizures by minutes in an animal model of temporal lobe epilepsy. J. Neurophysiol. *99*, 2431–2442.

Bragin, A., Azizyan, A., Almajano, J., Wilson, C.L., and Engel, J., Jr. (2005). Analysis of chronic seizure onsets after intrahippocampal kainic acid injection in freely moving rats. Epilepsia *46*, 1592–1598.

Cui, G., Jun, S.B., Jin, X., Luo, G., Pham, M.D., Lovinger, D.M., Vogel, S.S., and Costa, R.M. (2014). Deep brain optical measurements of cell type-specific neural activity in behaving mice. Nat. Protoc. *9*, 1213–1228.

de Lanerolle, N.C., Gunel, M., Sundaresan, S., Shen, M.Y., Brines, M.L., and Spencer, D.D. (1995). Vasoactive intestinal polypeptide and its receptor changes in human temporal lobe epilepsy. Brain Res. *686*, 182–193.

Ellender, T.J., Raimondo, J.V., Irkle, A., Lamsa, K.P., and Akerman, C.J. (2014). Excitatory effects of parvalbumin-expressing interneurons maintain hippocampal epileptiform activity via synchronous afterdischarges. J. Neurosci. *34*, 15208–15222.

Enger, R., Tang, W., Vindedal, G.F., Jensen, V., Johannes Helm, P., Sprengel, R., Looger, L.L., and Nagelhus, E.A. (2015). Dynamics of Ionic Shifts in Cortical Spreading Depression. Cereb. Cortex *25*, 4469–4476.

Grasse, D.W., Karunakaran, S., and Moxon, K.A. (2013). Neuronal synchrony and the transition to spontaneous seizures. Exp. Neurol. *248*, 72–84.

Gunaydin, L.A., Grosenick, L., Finkelstein, J.C., Kauvar, I.V., Fenno, L.E., Adhikari, A., Lammel, S., Mirzabekov, J.J., Airan, R.D., Zalocusky, K.A., et al. (2014). Natural neural projection dynamics underlying social behavior. Cell *157*, 1535–1551.

Hall, S., Hunt, M., Simon, A., Cunnington, L.G., Carracedo, L.M., Schofield, I.S., Forsyth, R., Traub, R.D., and Whittington, M.A. (2015). Unbalanced Peptidergic Inhibition in Superficial Neocortex Underlies Spike and Wave Seizure Activity. J. Neurosci. *35*, 9302–9314.

Hunt, R.F., Girskis, K.M., Rubenstein, J.L., Alvarez-Buylla, A., and Baraban, S.C. (2013). GABA progenitors grafted into the adult epileptic brain control seizures and abnormal behavior. Nat. Neurosci. *16*, 692–697.

Ko, F.J., Chiang, C.H., Liu, W.J., and Chiang, W. (1991). Somatostatin, substance P, prolactin and vasoactive intestinal peptide levels in serum and cerebrospinal fluid of children with seizure disorders. Gaoxiong Yi Xue Ke Xue Za Zhi *7*, 391–397.

Krook-Magnuson, E., Armstrong, C., Oijala, M., and Soltesz, I. (2013). On-demand optogenetic control of spontaneous seizures in temporal lobe epilepsy. Nat. Commun. *4*, 1376.

Kuner, T., and Augustine, G.J. (2000). A genetically encoded ratiometric indicator for chloride: capturing chloride transients in cultured hippocampal neurons. Neuron *27*, 447–459.

Lee, S., Kruglikov, I., Huang, Z.J., Fishell, G., and Rudy, B. (2013). A disinhibitory circuit mediates motor integration in the somatosensory cortex. Nat. Neurosci. *16*, 1662–1670.

Lodato, S., Tomassy, G.S., De Leonibus, E., Uzcategui, Y.G., Andolfi, G., Armentano, M., Touzot, A., Gaztelu, J.M., Arlotta, P., Menendez de la Prida, L., and Studer, M. (2011). Loss of COUP-TFI alters the balance between caudal ganglionic eminence- and medial ganglionic eminence-derived cortical interneurons and results in resistance to epilepsy. J. Neurosci. *31*, 4650–4662.

Lopantsev, V.E., and Taranenko, V.D. (1990). Paroxysmal afterpotentials and role of calcium-dependent potassium conductivity in neuronal activity of strychninized neocortex. Neuroscience *38*, 137–143.

Mantegazza, M., Rusconi, R., Scalmani, P., Avanzini, G., and Franceschetti, S. (2010). Epileptogenic ion channel mutations: from bedside to bench and, hopefully, back again. Epilepsy Res. *92*, 1–29.

Paz, J.T., and Huguenard, J.R. (2015). Microcircuits and their interactions in epilepsy: is the focus out of focus? Nat. Neurosci. *18*, 351–359.

Perreault, P., and Avoli, M. (1992). 4-aminopyridine-induced epileptiform activity and a GABA-mediated long-lasting depolarization in the rat hippocampus. J. Neurosci. *12*, 104–115.

Pi, H.-J., Hangya, B., Kvitsiani, D., Sanders, J.I., Huang, Z.J., and Kepecs, A. (2013). Cortical interneurons that specialize in disinhibitory control. Nature *503*, 521–524.

Potter, G.B., Petryniak, M.A., Shevchenko, E., McKinsey, G.L., Ekker, M., and Rubenstein, J.L.R. (2009). Generation of Cre-transgenic mice using Dlx1/Dlx2 enhancers and their characterization in GABAergic interneurons. Mol. Cell. Neurosci. *40*, 167–186.

Raol, Y.H., and Brooks-Kayal, A.R. (2012). Experimental models of seizures and epilepsies. In Molecular Biology and Translational Science, *Chapter 1* (Academic Press), pp. 57–82.

Scheyltjens, I., Laramée, M.-E., Van den Haute, C., Gijsbers, R., Debyser, Z., Baekelandt, V., Vreysen, S., and Arckens, L. (2015). Evaluation of the expression pattern of rAAV2/1, 2/5, 2/7, 2/8, and 2/9 serotypes with different promoters in the mouse visual cortex. J. Comp. Neurol. *523*, 2019–2042.

Shorvon, S.D. (2011). The etiologic classification of epilepsy. Epilepsia *52*, 1052–1057.

Staley, K.J., Soldo, B.L., and Proctor, W.R. (1995). Ionic mechanisms of neuronal excitation by inhibitory GABAA receptors. Science *269*, 977–981.

Toyoda, I., Fujita, S., Thamattoor, A.K., and Buckmaster, P.S. (2015). Unit Activity of Hippocampal Interneurons before Spontaneous Seizures in an Animal Model of Temporal Lobe Epilepsy. J. Neurosci. *35*, 6600–6618.

Truccolo, W., Donoghue, J.A., Hochberg, L.R., Eskandar, E.N., Madsen, J.R., Anderson, W.S., Brown, E.N., Halgren, E., and Cash, S.S. (2011). Single-neuron dynamics in human focal epilepsy. Nat. Neurosci. *14*, 635–641.

Wells, M.F., Wimmer, R.D., Schmitt, L.I., Feng, G., and Halassa, M.M. (2016). Thalamic reticular impairment underlies attention deficit in Ptchd1(Y/-) mice. Nature *532*, 58–63.

Neuron, Volume *93*

Supplemental Information

Dynamic, Cell-Type-Specific Roles for GABAergic Interneurons in a Mouse Model of Optogenetically Inducible Seizures

Sattar Khoshkhoo, Daniel Vogt, and Vikaas S. Sohal

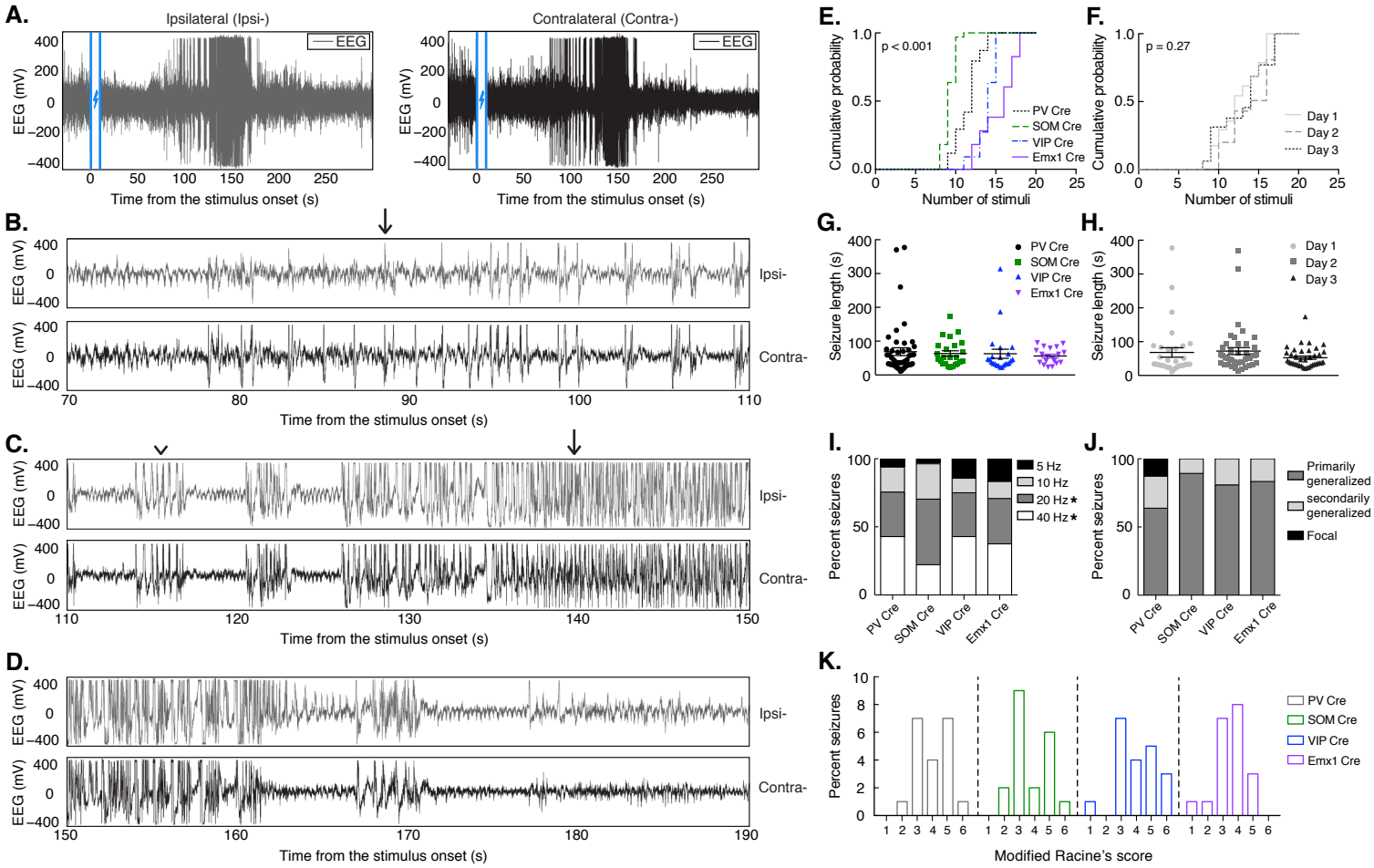

FIGURE S1 (Related to Figure 1)

(A) Example of bilateral EEG recordings during a primarily generalized seizure in a PV-Cre mouse. Time 0 marks the onset of the stimulus immediately preceding the seizure. Ipsilateral and contralateral refer to the placement of EEG screws with respect to the site of ChR2 stimulation. (B) Recordings from panel A, zoomed in to highlight the time around seizure initiation. Arrow points to a bilateral periodic discharge. (C) Recordings from panel A, zoomed in to highlight the period of seizure maintenance. Arrowhead points to a burst and arrow points to high amplitude, high frequency spikes. (D) Recordings from panel A, zoomed in to highlight seizure termination. (E) Cumulative probability of a seizure as a function of the number of stimuli delivered, across genotypes. (F) Cumulative probability of a seizure as a function of the number of stimuli delivered, across three days of experimentation. Data from each day includes PV-Cre, SOM-Cre, VIP-Cre, and Emx1-Cre mice.
(G) Seizure duration for each genotype. Each data point is derived from a single seizure. (H) Seizure duration across three days of experimentation. Each data point is derived from a single seizure. Data from each day includes PV-Cre, SOM-Cre, VIP-Cre, and Emx1-Cre mice.
(I) Percentage of seizures elicited by each stimulus frequency. (J) Classification of seizures into different types based on electrographic criteria.
(K) Classification of seizure intensity based on behavioral phenotypes using the modified Racine scale. All data show means ± SEM and are analyzed using one-way ANOVA and multiple comparisons test. In panels G through J, unless marked on the figure, there are no significant differences between different genotypes. $p<0.05$ (*).

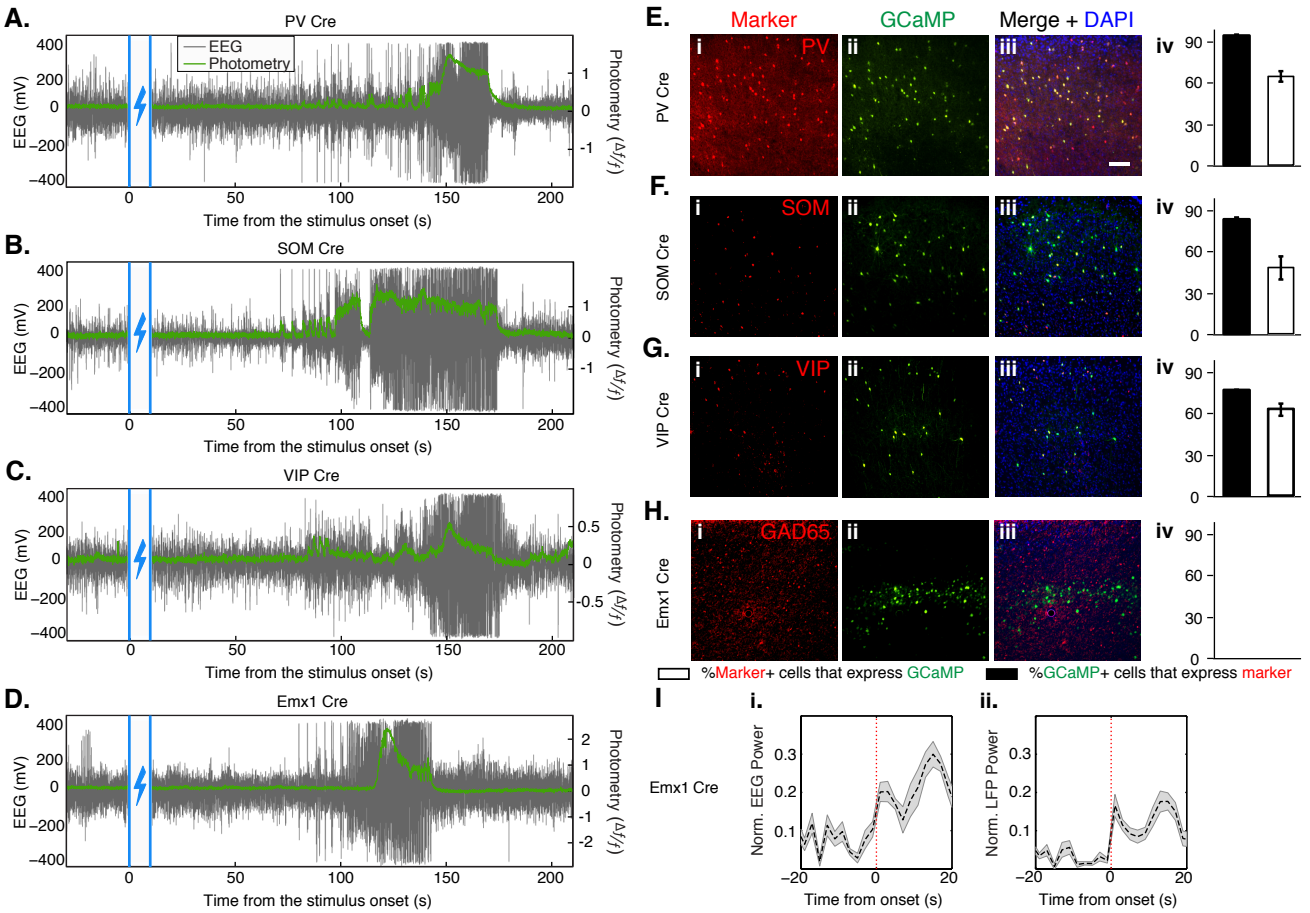

FIGURE S2 (Related to Figure 2)

(A-D) Examples of simultaneous EEG and photometry recordings from seizures in PV-Cre (A), SOM-Cre (B), VIP-Cre (C), and Emx1-Cre (D) mice. Time 0 marks the onset of the stimulus immediately preceding the seizure. (E) Adult coronal brain sections (25 μm) from area M1 were immuno-fluorescently labeled for PV (i) and visualized for native GCaMP expression (ii), driven by AAV-Syn-Flex-GCaMP6f-WPRE-SV40 injected in PV-Cre mice. Marker and GCaMP expression were overlapped (iii) and the proportion of transduced cells that express PV (black), or the total number of endogenous PV+ cells that were transduced (white), were quantified (iv). Scale bar in Eiii equals 100 μm. (F) The same as E, but for SOM-Cre mice with SOM as the marker. (G) The same as E, but for VIP-Cre mice with VIP as the marker. (H) The same as E, but for Emx1-Cre mice with GAD65 as the marker. (I) (i) Mean EEG power—normalized to the peak EEG power during each seizure—and (ii) mean LFP power—normalized to the peak LFP signal during each seizure—in Emx1-Cre mice, aligned to the time of seizure initiation (indicated by the dotted red line). All data show means ± SEM.

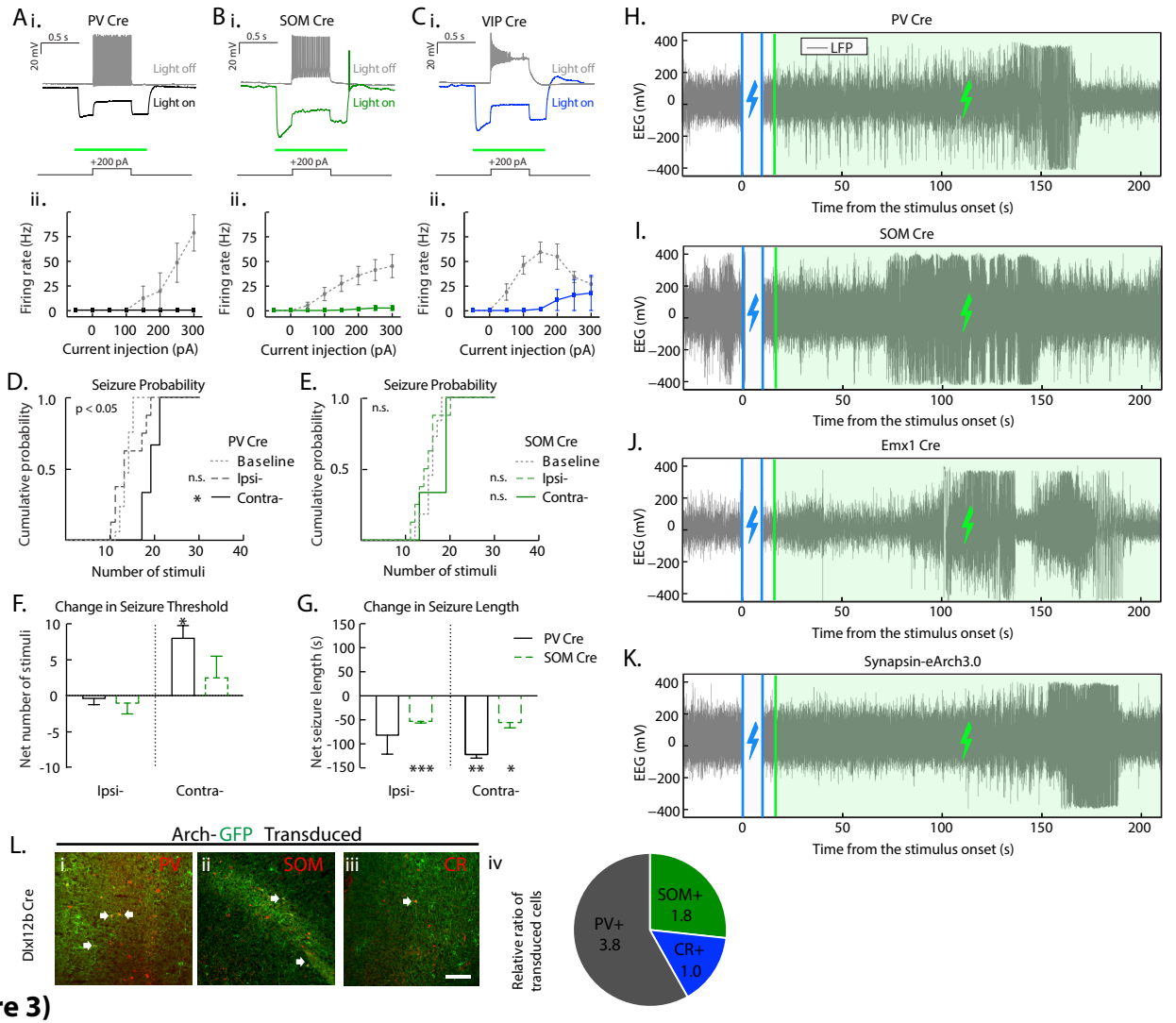

FIGURE S3 (Related to Figure 3)

(A-C) (i) Example of current-clamp responses of PV+ (A), SOM+ (B), and VIP+ (C) interneurons expressing eArch3.0-eYFP to injection of depolarizing current with (colored) and without (gray) illumination with green light. Schematic demonstrates timing of the depolarizing current injection and the green bar shows illumination with green light. (ii) F-I curves for PV+ (A), SOM+ (B), and VIP+ (C) interneurons expressing eArch3.0-eYFP with (colored) and without (gray) illumination with green light. (D-E) Cumulative probability for seizure induction as a function of the number of optogenetic stimuli delivered, in PV-Cre (D) and SOM-Cre (E) mice. There was no interneuron inhibition in the "Baseline" condition. "ipsi" and "contra" refer to optogenetic inhibition of ipsilateral or contralateral interneurons, respectively, as shown in Figure 3A. (F) Change in the number of stimuli required to induce the first seizure (seizure threshold) relative to baseline. Ipsi- and contra- refer to ipsilateral and contralateral interneuron inhibition, respectively, as shown in Figure 3A. (G) Change in seizure duration relative to baseline. Ipsi- and contra- refer to ipsilateral and contralateral interneuron inhibition, respectively, as shown in Figure 3A. (H-K) Example of LFP recordings during primarily generalized seizures with simultaneous inhibition of PV+ (H), SOM+ (I), Emx1+ (J), and synapsin-labeled (K) neurons at the site of LFP recording. Time "0" marks the onset of the stimulus immediately preceding the seizure. LFP recordings were made at the site of optogenetic inhibition, which was contralateral to the site of ChR2 stimulation. (L) Most transduced cells in Dlxl12b-Cre mice express PV or SOM, not calretinin (CR). All data show means ± SEM. Data in D and E are analyzed using ANOVA and multiple comparisons test. Data in F and G are analyzed using two-tailed t-tests. In F and G, there are no significant changes except where indicated. Not significant (n.s.), $p<0.05$ (*), $p<0.01$ (**), $p<0.001$ (***).

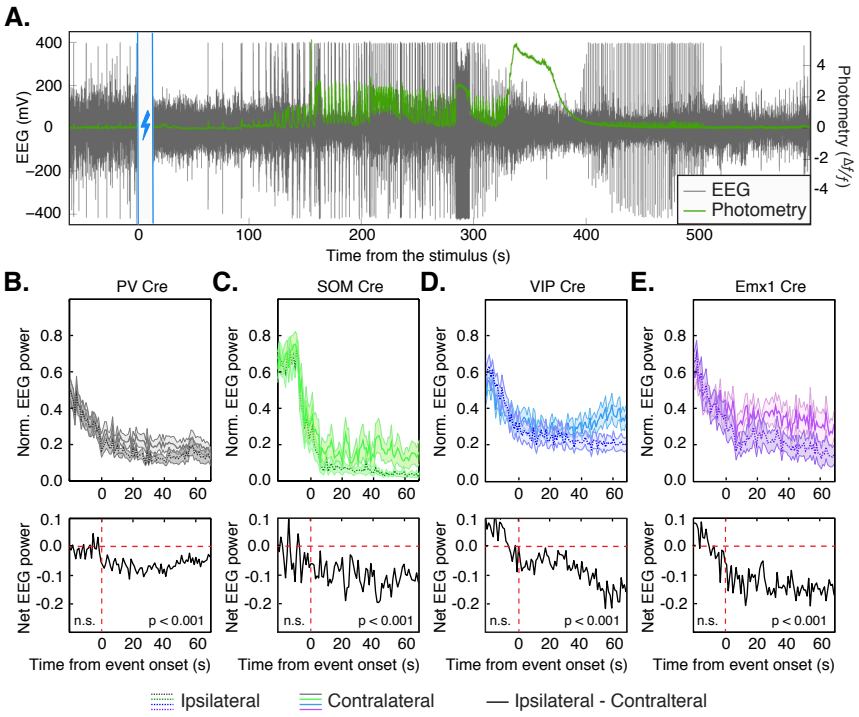

FIGURE S4 (Related to Figure 4)
(A) Example of simultaneous EEG and photometry recording of a CSD-like event that occurred midway during a seizure in a PV-Cre mouse. Time 0 indicates the beginning of the stimulus immediately preceding the seizure. (B-E) Mean EEG power in PV-Cre (B), SOM-Cre (C), VIP-Cre (D), and Emx1-Cre (E) mice aligned to the onset of each CSD-like event. Averages from the electrodes ipsilateral and contralateral to the photometry site have been included in the top panel. The trace in the bottom panel is the net difference in EEG power between the ipsilateral and contralateral electrodes. All data show means ± SEM and are analyzed using a one-tail paired t-test. Shading in the traces and error bars in the scatter plots are ± SEM. p-values in panels B through E are calculated before the onset of the CSD-like events and after the onset of the CSD-like events.

EXPERIMENTAL PROCEDURES

All experiments were conducted in accordance with procedures established by the Administrative Panels on Laboratory Animal Care at the University of California, San Francisco.

Animals

We used the following mice: B6;129P2-*Pvalb*$^{tm1(cre)Arbr}$/J (The Jackson Laboratory), B6N.Cg-Sst$^{tm2.1(cre)Zjh}$/J (The Jackson Laboratory), Vip$^{tm1(cre)Zjh}$/J (The Jackson Laboratory), B6.129S2-Emx1$^{tm1(cre)Krj}$/J (The Jackson Laboratory), and Tg(I12b-cre)1Jlr (The Jackson Laboratory). PV-Cre, SOM-Cre, VIP-Cre, and Emx-Cre mice were on a C57Bl6 background and DlxI12b-Cre mice were on a CD1 background. All mice were fed *ad libitum* and reared in normal lighting conditions (12/12 light/dark cycle).

Injection of virus for ChR2 expression

To express channelrhodopsin (ChR2), we used a previously described adeno-associated virus (AAV) that encodes ChR2-mCherry under the control of a CaMKIIα promoter (Sohal et al., 2009). It is important to note that the CaMKIIα1.3 promoter used here is only 82% specific to excitatory neurons, and also drives expression of other populations of neurons including some interneurons (Scheyltjens et al., 2015). Virus (from constructs contributed by Karl Deisseroth) was packaged by UNC Vector Core with serotype 5. Coordinates (in millimeters relative to the bregma) for injection into the primary motor cortex were 1.5 anteroposterior (AP), $\pm$1.3 to 1.5 mediolateral (ML), and –1.3 to –1.4 dorsoventral (DV). We injected 1.0 μL of AAV-CaMKIIα-ChR2-mCherry following previously-described procedures (Sohal et al., 2009) in either hemisphere (one injection per mouse). We then waited at least 5 weeks before beginning behavioral experiments.

Injection of virus for GCaMP6f expression

To express GCaMP6f in interneurons and excitatory neurons, we used an AAV vector that drivers the expression of Flex-GCaMP6f-WPRE-SV40 under the Syn promoter in PV-Cre, SOM-Cre (Taniguchi et al., 2011), VIP-Cre (Taniguchi et al., 2011), and Emx1::Cre (Gorski et al., 2002) mice. PV+, SOM+, and VIP+ interneurons account for the majority of interneurons in the cortex (Rudy et al., 2011). Virus (from Vivek Jayaraman, Rex A. Kerr, Douglas S. Kim, Loren L. Looger, Karel Svoboda from the GENIE Project, Janelia Farm Research Campus, Howard Hughes Medical Institute) was packaged by UPenn Vector Core with serotype AAV1. Coordinates (in millimeters relative to the bregma) for injection into the primary motor cortex were 1.5 AP, 1.5 ML, –1.4 DV. We injected 0.5 μL of AAV-Syn-Flex-GCaMP6f-WPRE-SV40 following previously-described procedures (Sohal et al., 2009), 3-4 weeks after AAV-CaMKIIα-ChR2-mCherry injection, in the hemisphere contralateral to the ChR2 injection site (one

injection per mouse). We then waited 2-3 weeks before beginning behavioral experiments.

Injection of virus for Arch expression

Interneuron inhibition experiments:
To express archaerhodopsin (Arch) in interneurons, we used an AAV vector that drivers the expression of DIO-eArch3.0-eYFP under the ubiquitous EF1α promoter in VIP-Cre and Dlx12b-Cre (Potter et al., 2009) mice. Virus (from constructs contributed by Karl Deisseroth) was packaged by UNC Vector Core with serotype AAV5. Coordinates (in millimeters relative to the bregma) for injection into the primary motor cortex were 1.5 AP, $\pm$1.5 ML, –1.4 DV. We injected 1.0 μL of AAV-EF1α-DIO-eArch3.0-eYFP or AAV-EF1α-DIO-eYFP (control) following previously-described procedures (Sohal et al., 2009) into both hemispheres (two injection per mouse), at the same time as the AAV-CaMKIIα-ChR2-mCherry injection. We then waited at least 5 weeks before beginning behavioral experiments.

Field inhibition experiments:
To express Arch in specific cell-types, we used an AAV vector that drivers the expression of DIO-eArch3.0-eYFP under the ubiquitous EF1α promoter in PV-Cre, SOM-Cre, and Emx-Cre mice. To express Arch in all cells, we used an AAV vector that drivers the expression of eArch3.0-eYFP under the ubiquitous Synapsin (Syn) promoter in PV-Cre mice. Virus (from constructs contributed by Karl Deisseroth) was packaged by UNC Vector Core with serotype AAV5. Coordinates (in millimeters relative to the bregma) for injection into the primary motor cortex were 1.5 AP, 1.5 ML, –1.4 DV. We injected 1.0 μL of AAV-EF1α-DIO-eArch3.0-eYFP or AAV-Syn-eArch30-eYFP following previously-described procedures (Sohal et al., 2009) into the hemisphere contralateral to the site of AAV-CaMKIIα-ChR2-mCherry injection. We then waited at least 4 weeks before beginning behavioral experiments.

EEG and fiber-optic cannula surgery for photometry

Surgeries were performed under isofluorane anesthesia in two stages. During the first surgery, AAV-CaMKIIα-ChR2-mCherry was injected in one hemisphere as described earlier, skin was proximated, and sutured (Coated vicryl suture, ETHICON Inc.). During the second surgery, 3-4 weeks later, AAV-Syn-Flex-GCaMP6f-WPRE-SV40 was injected in the opposite hemisphere as described earlier, then stainless steel skull screws for EEG recording (Pinnacle Technology, Inc.) and two fiber-optic cannulas (Doric Lenses, Inc.) were implanted intracranially. Two EEG recording electrodes were implanted at (in millimeters relative to the bregma) $-$0.75 AP, $\pm$3.0 ML (primary somatosensory cortex), a reference electrode was implanted at either $-$5.0 AP, 0 ML (cerebellum) or 5.0 AP, $-$1.0 ML (Olfactory bulb), and a ground electrode was implanted at $-$3.5 AP, $-$3.0 ML (primary visual cortex). One fiber-optic cannula for stimulation (200μm diameter, 0.22 NA, flat) was implanted at 1.5 AP, 1.5 ML, –1.2 DV above the

AAV-CaMKIIα-ChR2-mCherry injection site. One fiber-optic cannula for photometry (400μm diameter, 0.48 NA, flat) was implanted at 1.5 AP, 1.5 ML, –1.2 above the AAV-Syn-Flex-GCaMP6f-WPRE-SV40 injection site to capture emitted fluorescence from the calcium indicator and transmit it, via an optical fiber, to a photodetector (fiber photometry) (Cui et al., 2014; Gunaydin et al., 2014). EMG wires were fixed in the trapezius muscles as described before (Clegern et al., 2012), and EEG screws were attached to a 4 channel EEG/EMG headmount (Pinnacle Technology, Inc.) using conductive wires. Dental cement was used to fix the headmount and fiber-optic cannulas. Photometry experiments began at least 2 weeks after the surgery to allow time for optimal viral expression.

EEG and fiber-optic cannula surgery for interneuron inhibition

Surgeries were performed under isofluorane anesthesia. First AAV-CaMKIIα-ChR2-mCherry was injected in one hemisphere as described earlier, then AAV-EF1α-DIO-eArch3.0-eYFP or AAV-EF1α-DIO-eYFP were injected bilaterally as described earlier. Stainless steel skull screws for EEG recording (Pinnacle Technology, Inc.) and two fiber-optic cannulas (Doric Lenses, Inc.) were implanted intracranially. The EEG recording electrodes were implanted at (in millimeters relative to the bregma) -0.75 AP, ± 3.0 ML (primary somatosensory cortex), a reference electrode was implanted at -5.0 AP, 0 ML (cerebellum), and a ground electrode was implanted at -3.5 AP, -3.0 ML (primary visual cortex). Two fiber optic cannulas (200μm diameter, 0.22 NA, flat) were implanted at 1.5 AP, ± 1.5 ML, –1.2 DV above the injection sites. EEG screws were attached to a 4 channel EEG/EMG headmount (Pinnacle Technology, Inc.) using conductive wires. Dental cement was used to fix the headmount and fiber-optic cannulas. Seizure inhibition experiments began at least 5 weeks after the surgery to allow time for optimal viral expression.

EEG, LFP, and fiber-optic cannula surgery for field inhibition

Surgeries were performed under isofluorane anesthesia. First AAV-CaMKIIα-ChR2-mCherry was injected in one hemisphere as described earlier, then AAV-EF1α-DIO-eArch3.0-eYFP or AAV-Syn-eArch3.0-eYFP was injected in the contralateral hemiesphere as described earlier. Stainless steel skull screws for EEG recording (Pinnacle Technology, Inc.), one fiber-optic cannula (Doric Lenses, Inc.), and one optrode were implanted intracranially. We fabricated optrodes for simultaneous optogenetic inhibition and LFP recording using 100MΩ tungsten microelectrodes (Microprobes, Inc.) and fiber optic cannulas (200μm diameter, 0.22 NA, flat, Doric Lenses, Inc.). We attached one microelectrode to the tip of the fiber optic cannula using heat shrink and a veterinary tissue adhesive (3M, Inc.), such that the tip of the microelectode extended past the end of the fiber by ~200µm. The EEG recording electrodes were implanted at (in millimeters relative to the bregma) -0.75 AP, ± 3.0 ML (primary somatosensory cortex), a reference electrode was implanted at -5.0 AP, 0 ML (cerebellum), and a ground electrode was implanted at -3.5 AP, -3.0 ML (primary

visual cortex). One fiber optic cannula (200μm diameter, 0.22 NA, flat) was implanted at 1.5 AP, -1.5 ML, –1.2 DV above the ChR2 injection site. One optrode was implanted at 1.5 AP, 1.5 ML, –1.2 DV above the Arch injection site. EEG screws and the LFP microelectrode were attached to a 4 channel EEG/EMG headmount (Pinnacle Technology, Inc.) using conductive wires. Dental cement was used to fix the headmount and fiber-optic cannulas. Seizure inhibition experiments began at least 4 weeks after the surgery to allow time for optimal viral expression.

In vivo optogenetic seizure induction

A 473 nm blue laser (Opto Engine LLC) was used to stimulate ChR2 through a fiber-optic patchcord (Doric Lenses, Inc.) coupled to an implant. Each optical stimulus was 10 seconds in length and it was delivered every ~3 minutes to allow for the development of epileptiform discharges and to avoid the development of afterdepolarizations (Osawa et al., 2013). If epileptiform discharges developed during the inter-stimulus interval, no stimuli were delivered until a seizure developed or EEG activity and behavior returned to baseline. The frequency of each optical stimulus was varied sequentially between 5, 10, 20, and 40 Hz, and this was controlled using a function generator (Agilent 33210A Series Arbitrary Waveform Generator). The generated stimuli were square waves at 50% duty cycle, meaning while the number of laser pulsations changed for each stimulation cycle, the duration of illumination remained constant at ~5s per stimulation epoch. Light power at the tip of the fiber-optic was ~0.5 mW initially, then increased by 2-4 mW after each four stimuli to identify the minimum light intensity required for seizure induction. In other words, during optogenetic seizure induction no two stimuli had the same frequency and light power. Maintaining a constant stimulation power and frequency, as we attempted during the preliminary stages of our experiments, precluded consistent optogenetic seizure induction. We attributed this to some form of "habituation" of the neuronal circuit to the stimulus. However, due to cross-activation of GCaMP by the blue laser used for ChR2 stimulation, we were unable to precisely define the nature of such habituation using Ca^{2+} imaging. After every seizure, there was a minimum 5 minute rest period before resuming stimulation. Stimulation was only resumed when EEG activity and behavior returned to baseline. No more than 5 seizures were induced in one day. If a seizure did not spontaneously terminate within 10 minutes, animal was put under isofluorane anesthesia to break the seizure and no more experiments were done on that day.

In vivo seizure induction and photometry

Seizure induction was performed as described earlier. Simultaneous *in vivo* bulk calcium imaging (photometry) was conducted using the setup described before. The photometry signal was sampled at 800 Hz. TTL pulses generated by a function generators (Agilent 33210A Series Arbitrary Waveform Generator) were used to synchronize the EEG and photometry recordings.

In vivo seizure induction and interneuron inhibition

In experiments that included optogenetic inhibition, a 445 nm blue laser (Opto Engine LLC) was used to stimulate ChR2 through a fiber-optic patchcord (Doric Lenses, Inc.) coupled to an implant. We used a 445 nm laser instead of the previously used 473 nm laser to minimize cross-activation of Arch. Seizure induction was performed as described earlier. A 594 nm amber laser (Cobalt laser) was used to stimulate Arch in order to inhibit interneuron activity. These experiments were performed over three days and the only difference between experiments on different days was the presence of optogenetic inhibition of interneurons. No inhibition was delivered on day 1 (baseline). On days 2 and 3, inhibition was delivered either ipsilateral (-ipsi) or contralateral (-contra) to the side of ChR2 stimulation. Sometimes days 2 and 3 consisted of ipsilateral inhibition followed by contralateral inhibition (n=4 experiments), while in other cases the order was reversed (n=3 experiments). The amber light (constant, ~2mW at the tip of the optical fiber) was turned on 5 seconds after the end of the 10 second blue optical stimulus and turned off 30 seconds before the onset of the next optical stimulus. If a seizure developed, the amber light remained on until the seizure terminated (based on the EEG signal). Amber and blue lasers were controlled using a custom-written MATLAB function (MathWorks, Inc.) driving two function generators (Agilent 33210A Series Arbitrary Waveform Generator).

In vivo seizure induction for field inhibition experiments

A 445 nm blue laser (Opto Engine LLC) was used to stimulate ChR2 through a fiber-optic patchcord (Doric Lenses, Inc.) coupled to an implant. The 445nm laser was chosen, instead of 473nm, to minimize the cross-activation of eArch3.0. Seizure induction was performed as described earlier. A 594 nm amber laser (Cobalt laser) was used to activate arch. These experiments were performed over two days. No inhibition was delivered on day 1 (baseline). On days 2, inhibition was delivered contralateral (-contra) to the side of ChR2 stimulation. The amber light (constant, ~2mW at the tip of the optical fiber) was turned on 5 seconds after the end of the 10 second blue optical stimulus and turned off 30 seconds before the onset of the next optical stimulus. If a seizure developed, the amber light remained on until the seizure terminated (based on the EEG signal). Amber and blue lasers were controlled using a custom-written MATLAB function (MathWorks, Inc.) driving two function generators (Agilent 33210A Series Arbitrary Waveform Generator).

EEG and LFP recording

EEG and LFP were recorded at 2 kHz using a time-locked video EEG monitoring system (Pinnacle Technology, Inc.). A common reference was used for the ipsilateral and contralateral EEG electrodes and the LFP electrode.

Identifying seizure onset and termination

In order to identify seizure onset and termination, we used a custom-developed algorithm that took into account total EEG power and line length. First, mean EEG power and line length were measured using a 10 second moving window, calculated at 1-second intervals. Thresholds for EEG power and line length were set for seizure detection, based on following formulas:

$$P_{threshold} = \mu(P_{baseline}) + \sigma(P_{total}) \times m \qquad m = \frac{P_{max}}{P_{baseline}} \times 50$$

$$L_{threshold} = \mu(L_{baseline}) + \sigma(L_{total}) \times m \qquad m = \frac{L_{max}}{L_{baseline}} \times 3$$

These formulas were developed empirically. To detect a seizure, EEG power had to cross $P_{threshold}$ continuously for 10 seconds and $L_{threshold}$ had to cross the baseline for at least 60% of the time during that period. The time point at which $P_{threshold}$ was crossed was set as seizure onset and the time point when mean power fell bellow the threshold was set as seizure termination. This algorithm was effective in identifying seizure onset and termination in the majority of cases. However, in order to assure consistently throughout our analysis, all seizure onset and termination times were manually confirmed twice in a randomized fashion, blinded to the identity of the mouse, its genotype, and day of experiment. In ~50% of the cases small manual adjustments were made to these values. For most seizures, the times of initiation and termination could be unambiguously determined from EEG recordings. However, in <10% of cases where the exact time of seizure onset or termination was not clear, those seizure was not included in further analysis.

Classifying seizure types

Seizure classification was strictly based on electrographic criteria, using only the EEG signal. Based the parameters described earlier, seizures were identified in bilateral EEG recordings independently of each other. The time of seizure onset in two hemispheres was marked and compared. Seizures that only appeared in one hemisphere, were classified as focal seizures. Seizures that appeared >1s earlier in one hemisphere were marked as focal seizures with secondary generalization. Seizure that had <1s difference between the time of seizure onset in two hemispheres were categorized as primarily generalized.

Semi-quantitative characterization of seizure phenotypes

We used a modified Racine scale (Singh et al., 2016) that divides seizure phenotypes based on severity into seven different categories: stage 0-no response; stage 1-hyperactivity, restlessness and vibrissae twitching; Stage 2-head nodding, head clonus and myoclonic jerks; Stage 3-unilateral or bilateral limb clonus; Stage 4-forelimb clonic

seizures; Stage 5-generalized clonic seizures with falling; Stage 6-appearance of tonic extension; and Stage 7-death. Since no animals died during these experiments, we removed stage 7 from our scale. Based on the parameters described earlier, we first identified seizures in PV-Cre, SOM-Cre, VIP-Cre, and Emx-Cre mice based on their electrographic features on bilateral EEG recordings. Then, video recordings from these electrographically identified seizures were viewed by a scorer blind to the mouse genotype. Each seizure was assigned a score from the modified Racine scale based on the maximum intensity of behavioral seizure characteristics reached during the seizure.

Identifying the onset of CSD-like events

The onset of these events were manually determined twice in a randomized fashion, blinded to the identity of the mouse, its genotype, and day of experiment. Given the stereotyped features of CSD-like events on photometry, first these events were easily identified, then the point at which the initial upslope started was marked as the time of onset. CSD peak was determined by finding the maximum photometry value during each event.

EEG and photometry analysis

All analyses were performed using custom-written and built-in MATLAB (MathWorks, Inc.) functions. The EEG signal was downsampled to 800 Hz in order to match the photometry sampling rate. TTL pulses were used to align EEG and photometry recordings.

To generate the aggregate EEG and photometry plots, total EEG power was calculated in one second bins. The photometry recording was downsampled to achieve the same number of data points. EEG and photometry recordings were normalized by dividing each trace by its maximum value. Then they were aligned based on the time of seizure onset or termination, and averaged. Only seizures that had a minimum duration of 30 seconds were included in this analysis. To generate the plots showing averaged activity relative to the time of seizure termination, we excluded seizures that did not terminate spontaneously. Seizures that had CSD-like events within the averaging window were also excluded.

To generate the compressed-time plots, total EEG power was calculated in one second bins. The photometry recording was downsampled to yield the same number of data points. EEG and photometry recordings were normalized by dividing each trace by its maximum value. Then both normalized EEG and photometry signals were downsampled to the duration of the smallest seizure, and averaged. Seizures that were shorter than 30 seconds, did not terminate spontaneously, or had CSD-like events within the averaging window were excluded from this analysis.

To maintain consistency with the photometry results, we only used the recordings from the EEG electrode contralateral to the stimulation site for analysis of seizure inhibition experiments. However, only generalized seizures were included.

To generate the aggregate CSD plots, total EEG power was calculated in one second bins. The photometry recording was downsampled to achieve the same number of data points. EEG and photometry recordings were normalized by dividing each trace by its maximum value. Then they were aligned based on the time of CSD onset or termination, and averaged.

Analysis of seizure threshold and duration

All analyses were performed using custom-written and built-in MATLAB (MathWorks, Inc.) functions. The EEG signal was downsampled to 800 Hz. Seizure detection was performed as described earlier. To calculate seizure probability and threshold, all seizures were included. For seizure duration analysis, however, only seizures that had identifiable onset and termination times were included. To generate plots showing changes in seizure threshold, the mean number of stimuli required to induce the first seizure on day 1 (baseline) was subtracted from the number of stimuli required to induce the first seizure on days 2 and 3. To generate plots demonstrating change in seizure duration, the mean duration of seizures on day 1 (baseline) was subtracted from the durations on days 2 and 3.

Slice preparation

We cut 250μm thick coronal slices from 8- to 10- week old mice of either sex in a chilled slicing solution in which Na^+ was replaced by sucrose. Then we incubated the slices in warmed cerebrospinal fluid (ACSF) at 30°C–31°C for 1 hour before being used for recording. ACSF contained (in mM): 126 NaCl, 26 $NaHCO_3$, 2.5 KCl, 1.25 NaH_2PO_4, 1 $MgCl_2$, 2 CaCl, and 10 glucose. We secured the slices via a harp along the midline.

Intracellular recording

We identified neurons transfected with AAV-EF1α-DIO-eArch3.0-eYFP based the expression of the fluorescent tag. Somatic whole-cell patch recordings were obtained from visually identified cells in layer 5 of primary motor cortex using differential contrast video microscopy on an upright microscope (BX51WI; Olympus). Recordings were made using a Multiclamp 700A (Molecular Devices). Patch electrodes (tip resistance = 2–6 MOhms) were filled with the following (in mM): 130 K-gluconate, 10 KCl, 10 HEPES, 10 EGTA, 2 MgCl, 2 MgATP, and 0.3 NaGTP (pH adjusted to 7.3 with KOH). All recordings were at 32.5±1°C. Series resistance was usually 10–20 MΩ, and experiments were discontinued above 30 MΩ.

Analysis of cellular inhibition with Arch

Firing rate vs. input current (F-I curve) was calculated based on the current clamp responses to a series of 500 msec current pulse injections from -50 to 500 pA in 50 pA increments. Then, the same protocol was repeated in each cell, this time with a constant 532nm light source (1mW) illuminating the slice from 250 msec before to 250 msec after the current step and a new F-I curve was calculated based on that.

Immuno-fluorescence and quantification of virally-transduced Cre+ brains

Coronal, 25 μm, brain sections were generated, then cells from the primary motor cortex or the PFC were visualized for native GCaMP fluorescence and for multiple GABAergic markers. GABAergic markers included GAD65, PV, SOM, VIP, and CR. To determine the specificity of Cre-dependent viral transduction, the proportion of GCaMP+ cells that co-labeled with particular markers was analyzed. In addition, the efficiency of endogenous cells that expressed the Cre-dependent reporter (GCaMP+) was determined by calculating the proportion of endogenous marker+ cells that were GCaMP+. The latter analysis was done by counting all the co-labeled GCaMP+/marker+ cells and dividing by the total marker+ cells in a 10x objective field of view.

Statistical analysis

All statistical analyses were performed using custom-written and built-in MATLAB (MathWorks, Inc.) functions. We used two-tailed Student's t-test to compare paired observations and one-way ANOVA with Tukey-Kramer multiple comparisons test if there were unpaired observations, unless otherwise specified. To compare cumulative probability distributions, portions of the distribution corresponding to probabilities of zero (no seizure) were not included in the statistical analysis. Error bars indicate ± 1 SEM.

Supplemental References

Clegern, W.C., Moore, M.E., Schmidt, M.A., and Wisor, J. (2012). Simultaneous electroencephalography, real-time measurement of lactate concentration and optogenetic manipulation of neuronal activity in the rodent cerebral cortex. J. Vis. Exp. JoVE e4328.

Cui, G., Jun, S.B., Jin, X., Luo, G., Pham, M.D., Lovinger, D.M., Vogel, S.S., and Costa, R.M. (2014). Deep brain optical measurements of cell type-specific neural activity in behaving mice. Nat. Protoc. *9*, 1213–1228.

Gorski, J.A., Talley, T., Qiu, M., Puelles, L., Rubenstein, J.L.R., and Jones, K.R. (2002). Cortical excitatory neurons and glia, but not GABAergic neurons, are produced in the Emx1-expressing lineage. J. Neurosci. Off. J. Soc. Neurosci. *22*, 6309–6314.

Gunaydin, L.A., Grosenick, L., Finkelstein, J.C., Kauvar, I.V., Fenno, L.E., Adhikari, A., Lammel, S., Mirzabekov, J.J., Airan, R.D., Zalocusky, K.A., et al. (2014). Natural neural projection dynamics underlying social behavior. Cell *157*, 1535–1551.

Osawa, S.-I., Iwasaki, M., Hosaka, R., Matsuzaka, Y., Tomita, H., Ishizuka, T., Sugano, E., Okumura, E., Yawo, H., Nakasato, N., et al. (2013). Optogenetically induced seizure and the longitudinal hippocampal network dynamics. PloS One *8*, e60928.

Potter, G.B., Petryniak, M.A., Shevchenko, E., McKinsey, G.L., Ekker, M., and Rubenstein, J.L.R. (2009). Generation of Cre-transgenic mice using Dlx1/Dlx2 enhancers and their characterization in GABAergic interneurons. Mol. Cell. Neurosci. *40*, 167–186.

Rudy, B., Fishell, G., Lee, S., and Hjerling-Leffler, J. (2011). Three groups of interneurons account for nearly 100% of neocortical GABAergic neurons. Dev. Neurobiol. *71*, 45–61.

Scheyltjens, I., Laramée, M.-E., Van den Haute, C., Gijsbers, R., Debyser, Z., Baekelandt, V., Vreysen, S., and Arckens, L. (2015). Evaluation of the expression pattern of rAAV2/1, 2/5, 2/7, 2/8, and 2/9 serotypes with different promoters in the mouse visual cortex. J. Comp. Neurol. *523*, 2019–2042.

Singh, P., Singh, D., and Goel, R.K. (2016). Protective effect on phenytoin-induced cognition deficit in pentylenetetrazol kindled mice: A repertoire of Glycyrrhiza glabra flavonoid antioxidants. Pharm. Biol. *54*, 1209–1218.

Sohal, V.S., Zhang, F., Yizhar, O., and Deisseroth, K. (2009). Parvalbumin neurons and gamma rhythms enhance cortical circuit performance. Nature *459*, 698–702.

Taniguchi, H., He, M., Wu, P., Kim, S., Paik, R., Sugino, K., Kvitsiani, D., Kvitsani, D., Fu, Y., Lu, J., et al. (2011). A resource of Cre driver lines for genetic targeting of GABAergic neurons in cerebral cortex. Neuron *71*, 995–1013.